RSC Advances

PAPER

View Article Online
View Journal | View Issue

Cite this: *RSC Adv.*, 2021, **11**, 25497

Rational synthesis of a hierarchical Mo_2C/C nanosheet composite with enhanced lithium storage properties†

Xin Yue, Minglei Cao,* Limeng Wu, Wei Chen, Xingxing Li, Yanan Ma and Chuankun Zhang*

Transition metal carbides have been studied extensively as anode materials for lithium-ion batteries (LIBs), but they suffer from sluggish lithium reaction kinetics and large volume expansion. Herein, a hierarchical Mo_2C/C nanosheet composite has been synthesized through a rational pyrolysis strategy, and evaluated as an anode material with enhanced lithium storage properties for LIBs. In the hierarchical Mo_2C/C nanosheet composite, large numbers of Mo_2C nanosheets with a thickness of 40–100 nm are uniformly anchored onto/into carbon nanosheet matrices. This unique hierarchical architecture can provide favorable ion and electron transport pathways and alleviate the volume change of Mo_2C during cycling. As a consequence, the hierarchical Mo_2C/C nanosheet composite exhibits high-performance lithium storage with a reversible capacity of up to 868.6 mA h g^{-1} after 300 cycles at a current density of 0.2 A g^{-1}, as well as a high rate capacity of 541.8 mA h g^{-1} even at 5.0 A g^{-1}. More importantly, this hierarchical composite demonstrates impressive cyclability with a capacity retention efficiency of 122.1% over 5000 successive cycles at 5.0 A g^{-1}, which surpasses the cycling properties of most other Mo_2C-based materials reported to date.

Received 16th May 2021
Accepted 13th July 2021

DOI: 10.1039/d1ra03822b

rsc.li/rsc-advances

Introduction

Lithium-ion batteries (LIBs) have become one of the most important power sources, with applications from intelligent electronic devices and electric vehicles to grid-scale energy storage systems.[1–3] However, graphite, a most common commercial anode material for LIBs, is far from satisfactory due to its low theoretical capacity of 372 mA h g^{-1}, which is unable to meet the ever-increasing energy demand. Furthermore, graphite exhibits a short cycling life and severe safety issues arising from the formation of unstable SEI layers and lithium dendrites during cycling.[4–6] Over the last decade, transition metal oxides and sulfides have been considered as promising alternative anode materials for LIBs on account of their large theoretical capacity, high electrochemical reactivity and abundant natural resources.[7–10] Nevertheless, they suffer from inferior rate capability and rapid capacity fading because of their large volume change and poor electronic conductivity. Hence, it is highly desirable to develop advanced anode materials simultaneously with high capacity, superior rate capability and long-term cyclability for high-performance LIBs.

In recent years, transition metal carbides have been studied extensively as anode materials for LIBs.[11–13] Specifically, molybdenum carbide (Mo_2C) have received much attention in light of its large theoretical capacity, favorable electric conductivity, as well as good chemical and mechanical stability.[14–16] However, the sluggish lithium-ion transport kinetics and large volume expansion inevitably lead to poor rate performance and rapid capacity fading for this material. To tackle these challenges, one of the most effective methods is to design and construct the composites of Mo_2C and carbon, in which the volume expansion of Mo_2C can be relieved, as well as the charge transport properties can be significantly improved. For instance, Zhu *et al.*[17] reported Mo_2C/N-doped carbon mesoporous heteronanowires as suitable anode materials for LIBs, manifesting a reversible capacity of 941.1 mA h g^{-1} over 50 cycles at 0.1 A g^{-1}. Lu and co-workers[18] synthesized porous N,P co-doped Mo_2C/C nanosheets through calcining a chitosan–Mo composite hydrogel. The carbon nanosheet matrix can facilitate fast ion and electron transports and mitigate the volume expansion of Mo_2C during cycling. Mo_2C@C core–shell nanocrystals on 3D graphene hybrid aerogel was successfully synthesized and studied as LIBs anode material,[19] which retained a charge capacity of 1089.8 mA h g^{-1} over 100 cycles at 0.1 A g^{-1} and achieved a high rate capacity of 623.5 mA h g^{-1} at 5 A g^{-1}. These previous works have verified the potential of employing Mo_2C/C composites as anode materials for high-performance LIBs, whereas their cycling performance should be further improved. Hence, more researches should be devoted to enhance the cycling performance of Mo_2C/C composites by

School of Sciences, Hubei University of Automotive Technology, Shiyan 442002, P. R. China. E-mail: cml07114052@163.com; zhangchk_lx@huat.edu.cn

† Electronic supplementary information (ESI) available. See DOI: 10.1039/d1ra03822b

optimizing the morphology and architecture of Mo_2C/C composites, thus achieving robust lithium reaction kinetics and simultaneously alleviating the volume expansion of Mo_2C. Meanwhile, it is of significant importance to develop more effective and economical methods to synthesize the Mo_2C/C composites.

In this report, Mo_2C/C nanosheet composites were fabricated with a rational pyrolysis method using sodium chloride (NaCl) as templates. The cubic NaCl crystals can easily self-assemble and create a 2D spatial confinement to obtain the Mo_2C/C nanosheet composites. By optimizing the carbon content of the composites, the product (denoted as Mo_2C/C-2) presents a unique hierarchical architecture, in which Mo_2C nanosheets uniformly grow onto/into carbon nanosheets matrices. This architecture endows the Mo_2C/C-2 with several structural and kinetic advantages for electrochemical lithium storage, such as good structural integrality, slight volume expansion, and fast ion and electron transport properties. Hence, the Mo_2C/C-2 demonstrates an initial discharge capacity of up to 1057.3 mA h g^{-1} at 0.2 A g^{-1}, and retains a reversible capacity of 532.1 mA h g^{-1} (122.1% capacity retention efficiency) after 5000 consecutive cycles at 5.0 A g^{-1}. It is worth noting that the outstanding cycle life of the hierarchical Mo_2C/C nanosheet composite surpasses the cycling properties of most other Mo_2C-based materials reported to date.

Experimental

Preparation of hierarchical Mo_2C/C nanosheet composite

In a typical synthesis, 3 mmol of $Na_2MoO_4 \cdot 2H_2O$, 1 mmol of $C_6H_{12}O_6$, and 25 mmol of NaCl were dissolved in 60 mL deionized water through magnetic stirring. Subsequently, the above mixed solution was placed in an oven and heated rapidly to 80 °C until fully evaporation of the water. The resultant brown precipitate was grinded into very fine powders and then sintered at 800 °C for 2 h with a ramp rate of 5 °C min^{-1} in Ar atmosphere. Finally, the final product (Mo_2C/C-2) was collected by centrifugation and rinsed in distilled water and ethanol, followed by drying at 80 °C under vacuum. For comparison, the Mo_2C/C nanosheet composites synthesized through the identical procedures but using 0.5 and 2 mmol of $C_6H_{12}O_6$ were marked as Mo_2C/C-1 and Mo_2C/C-3, respectively. Additionally, pure carbon (denoted as p-C) and Mo_2C/C composite (Mo_2C/C-4) were prepared through the identical procedures without use of $Na_2MoO_4 \cdot 2H_2O$ and NaCl, respectively.

Material characterization

The phase composition and crystallinity of the as-prepared Mo_2C/C composites were characterized by X-ray diffraction (XRD) measurement using an X'Pert 3 X-ray diffractometer (Cu Kα radiation, 2θ range of 20–80°). A Thermo scientific FT-Raman spectrometer (Nd-line laser source with 532 nm wavelength) was used for collecting the Raman spectra of the samples. The carbon contents in the as-prepared Mo_2C/C composites were measured by thermogravimetric analysis (TGA, Q600) in air. X-ray photoelectron spectroscopy (XPS, Thermo Scientific K-Alpha) measurements were conducted to investigate the elemental composition and surface chemical state of the samples. The morphological and structural features of the obtained products were studied using Field emission scanning electron microscopy (FSEM, FEI Nova NanoSEM 450) and transmission electron microscopy (TEM, FEI Titan G^2 60–300), equipped with energy dispersive spectroscope (EDS).

Electrochemical measurements

The working electrode was made by pasting the slurry consisting of 80 wt% Mo_2C/C nanosheet composites, 10 wt% acetylene black, and 10 wt% polytetrafluoroethylene onto copper foil using *N*-methyl-2-pyrrolidinone as a solvent. The coated copper foils were dried overnight in a vacuum oven at 80 °C, and then cut into 14 mm circular disks. The average mass loading of the active materials (Mo_2C/C nanosheet composites) was around 1.2 mg cm^{-2}. The CR-2032 coin cells were fabricated in an Ar-filled dry glove box using metallic lithium foils as the counter/reference electrodes and Celgard 2400 polypropylene membranes as the separators. The electrolyte consists of 1 M $LiPF_6$ in a solution of EC and DEC in a 1 : 1 volume ratio. Galvanostatic charge/discharge tests were conducted in the potential window of 0.01–3.0 V (*vs.* Li/Li^+) on a LAND-CT2001C tester. Cyclic voltammetry (CV) curves were obtained using an electrochemical workstation (CHI660E) at different scanning rates within the potential range from 0.01 to 3.0 V. Electrochemical impedance spectroscopy (EIS) measurements were performed on the CHI660E workstation in the frequency range between 100 kHz and 10 mHz with a sine wave of 5 mV.

Results and discussion

Material preparation and characterization

As schematically illustrated in Fig. 1, the preparation route of hierarchical Mo_2C/C nanosheet composite mainly involves

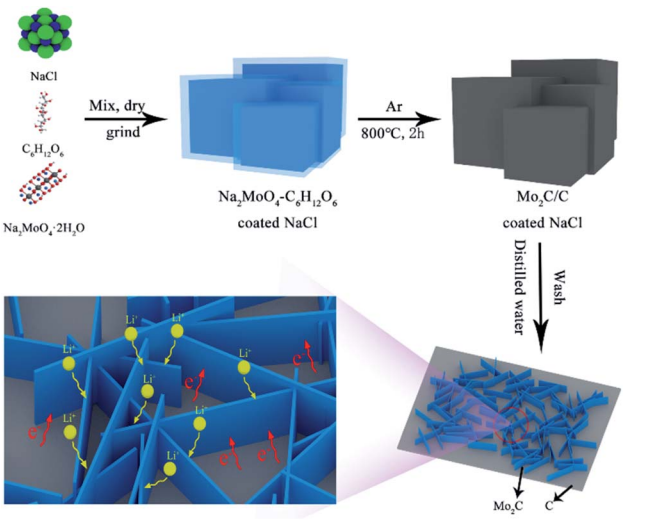

Fig. 1 Schematic illustration of fabrication of hierarchical Mo_2C/C nanosheet composite.

three main steps. The first step is formation of the intermediate complex of Na_2MoO_4–$C_6H_{12}O_6$ coated NaCl by dissolving these chemicals in deionized water and then completely evaporating the water. Subsequently, the intermediate product is annealed under Ar atmosphere at 800 °C to obtain the composite of Mo_2C/C coated NaCl. Finally, the NaCl templates are removed by wash with water, thus resulting in the formation of hierarchical Mo_2C/C nanosheet composite. Owing to its kinetic and structural merits, the hierarchical Mo_2C/C nanosheet composite could exhibit high Li^+ accessibility, favorable electron transport pathways and good structural integrality.

Fig. 2a displays the XRD patterns of the various Mo_2C/C composites. Sharp diffraction peaks can be seen for all these three samples, which indicates good crystallinity of the Mo_2C/C composites. The diffraction peaks at 2-theta of 34.4, 37.9, 39.4, 52.1, 61.6, 69.6, 72.5, 74.7 and 75.6° can be assigned to the (100), (002), (101), (102), (110), (103), (200), (112) and (201) crystal planes of hexagonal Mo_2C (JCPDS no. 35-0787), respectively.[20,21] Obviously, the peak intensity becomes weaker with increasing the carbon content in the composites. In addition, no diffraction peak pertaining to carbon species is detected in the XRD patterns, thus implying the carbon is in amorphous state. To get a deeper understanding of the carbon structure in the Mo_2C/C composites, Raman characterization were performed. As seen in Fig. 2b, all the products reveal two obvious Raman peaks and the peak intensity grows stronger with the increase of carbon content. The characteristic peaks located at about 1345 and 1592 cm^{-1} can be attributed to the D and G bands of the amorphous carbon, respectively. Specifically, the D band associates with the disordered planes and defects in graphitic structure, while the G band originates from the sp^2-hybridized carbon atoms.[22,23] Herein, the intensity ratios (I_D/I_G) of D band to G band are 1.32 for Mo_2C/C-1, 1.06 for Mo_2C/C-2, and 1.04 for Mo_2C/C-3, which manifest the presence of abundant carbon component with rich defects.

The elemental composition and surface chemical state of Mo_2C/C-2 were analyzed by XPS. Fig. S1† shows the XPS survey spectrum, which confirms the presence of Mo, C and O elements within this material. As depicted in Fig. 2c, the high-resolution Mo 3d spectrum can be fitted into three doublets. The peaks with binding energies at 228.6 and 231.7 eV are assigned to Mo^{2+} from Mo_2C, and the other two pairs of peaks are ascribed to Mo^{4+} (229.3/233.1 eV) and Mo^{6+} (232.6/235.8 eV) in molybdenum oxidized phases associated with the surface oxidation of Mo_2C.[20,24] The high-resolution spectrum of C 1s (Fig. 2d) contains three peaks with binding energies at 283.6, 285.3, and 288.0 eV, which can be attributed to C–Mo, C–C, and O–C=O, respectively.[20,25] The carbon contents in the various Mo_2C/C composites are determined based on TGA. As shown in Fig. S2,† the TGA curves for all the three samples display a weight loss in the temperature range from 370 to 500 °C, which can be attributed to the combustion of the carbon component. Above 600 °C, no weight change is observed in all the TGA curves, indicating the Mo_2C is fully converted into MoO_3 in air.[16,24] Based on the thermal properties of the Mo_2C/C composites, the carbon contents can be calculated using formula (S1) (see in ESI†). Hence, the carbon contents in Mo_2C/C-1, Mo_2C/C-2, and Mo_2C/C-3 are 3.8%, 14.0%, and 22.2%, respectively.

Fig. 3 presents the SEM images of the various Mo_2C/C composites. Numerous small Mo_2C nanosheets and large carbon nanosheet matrices are clearly observed, forming Mo_2C/C nanosheet composites. The thickness of the Mo_2C nanosheets is within the range of 40–100 nm. As seen in Fig. 3a and d, the Mo_2C nanosheets agglomerate into a sphere-like structure for Mo_2C/C-1, this could be attributed to the low carbon content in this sample. Owing to the suitable amount of carbon in Mo_2C/C-2 (Fig. 3b and e), the Mo_2C nanosheets uniformly grow onto/into the carbon nanosheet matrices. This unique architecture could significantly enhance electrochemical lithium storage properties in consideration of the favourable ion and electron transport pathways and good structural integrality. With further increasing the carbon content, the thickness of the carbon nanosheet matrices becomes thicker and the Mo_2C nanosheets agglomerate into sphere-like structure on the carbon matrices again (Fig. 3c and f). According to the SEM analysis, it can be concluded that the carbon content plays a vital role in

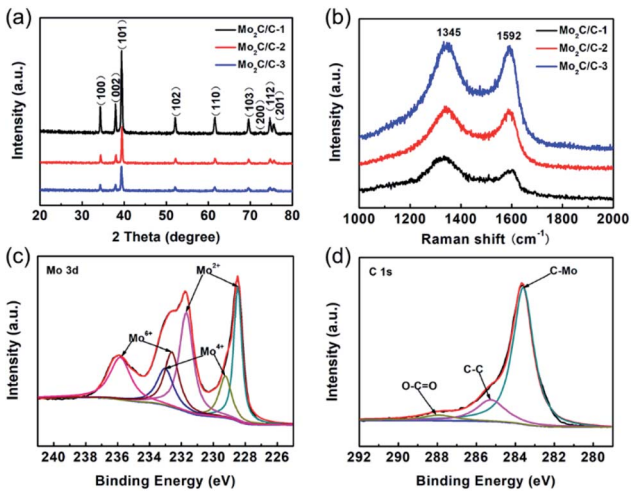

Fig. 2 (a) XRD patterns and (b) Raman spectra of various Mo_2C/C composites; high-resolution XPS spectra of (c) Mo 3d and (d) C 1s.

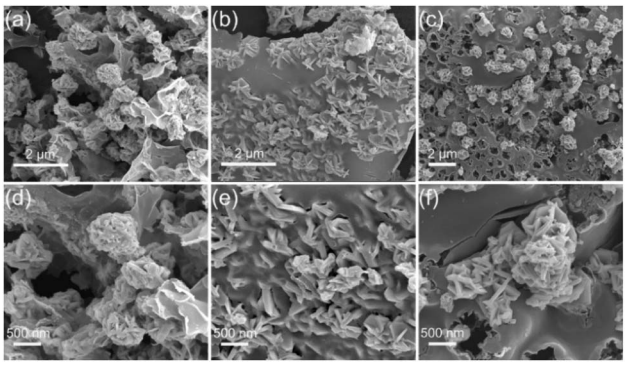

Fig. 3 SEM images of (a and d) Mo_2C/C-1, (b and e) Mo_2C/C-2, and (c and f) Mo_2C/C-3 with different magnification.

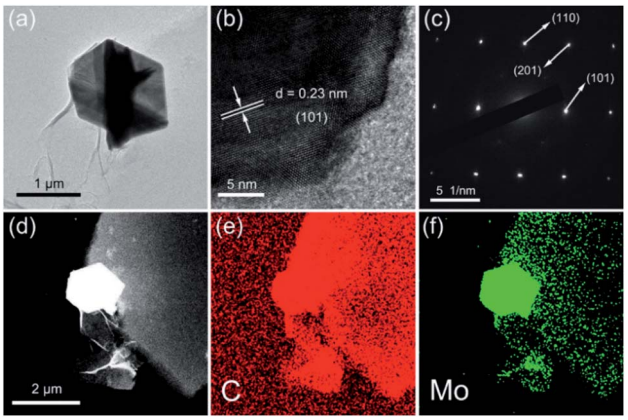

Fig. 4 (a) TEM and (b) HR-TEM images of Mo_2C/C-2; (c) SAED pattern of the Mo_2C/C-2; EDS mapping images of (d) the Mo_2C/C-2 and the elements of (e) C, (f) Mo, respectively.

controlling the morphology of Mo_2C/C composites, thus largely affects the lithium storage properties.

Further insights into the morphology and microstructure of Mo_2C/C-2 were elucidated by TEM. As displayed in Fig. 4a, the Mo_2C nanosheets are interconnected to anchored on carbon nanosheet matrices. The high resolution TEM (HR-TEM) image of the edge of Mo_2C nanosheet is shown in Fig. 4b, in which well-crystallized structure of the Mo_2C nanosheet can be clearly observed. The lattice fringe with an interplanar spacing of 0.23 nm is in agreement well with the (101) plane of Mo_2C.[24,25] The carbon matrices show no lattice fringe, being a further proof of their amorphous state. As seen in Fig. 4c, the SAED pattern reveals single crystalline nature of the Mo_2C nanosheets, and the lattice spaces are well matched to the (101), (110) and (201) planes of the Mo_2C phase.[18,21] Additionally, the EDS mapping images are displayed in Fig. 4d–f, which demonstrate the Mo_2C nanosheets are fixed on carbon nanosheets matrice and the hierarchical nanosheet composite consists of the elements of Mo and C.

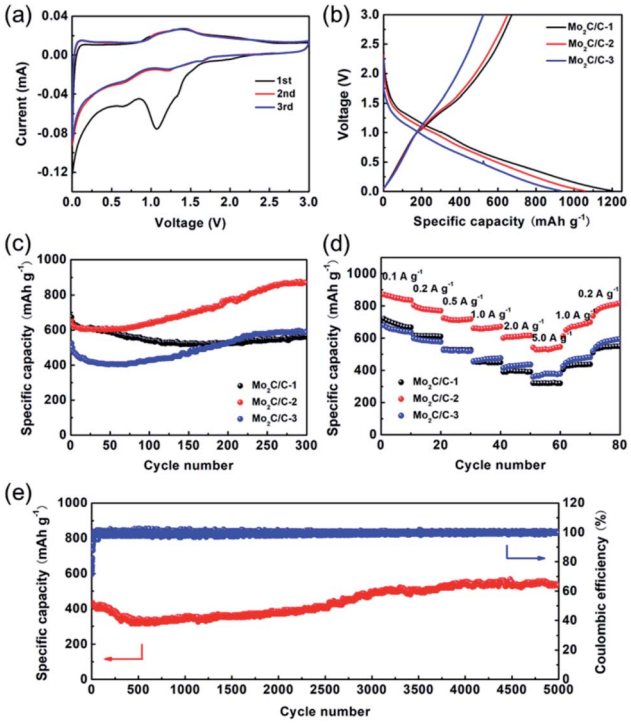

Fig. 5 (a) Initial three CV curves of Mo_2C/C-2 at the scan rate of 0.1 mV s^{-1}; (b) initial galvanostatic profiles of Mo_2C/C-1, Mo_2C/C-2 and Mo_2C/C-3 at the current density of 0.2 A g^{-1}, (c) cycling performance comparison of Mo_2C/C-1, Mo_2C/C-2 and Mo_2C/C-3 at the current density of 0.2 A g^{-1}; (d) rate performance of Mo_2C/C-1, Mo_2C/C-2 and Mo_2C/C-3 at various current densities from 0.1 to 5.0 A g^{-1}; (e) long-term cycling performance of Mo_2C/C-2 at the high current density of 5.0 A g^{-1}.

Electrochemical and kinetic characteristics

We then evaluated the lithium storage performances of the Mo_2C/C nanosheet composites in half-cells using metallic lithium foils as counter/reference electrodes. Fig. 5a depicts the initial three CV curves of Mo_2C/C-2 at 0.1 mV s^{-1}. In the first CV curve, a prominent cathodic peak (~1.07 V) is observed, which is related to the formation of SEI and conversion reaction of Mo_2C to Mo. In addition, the cathodic peak at about 0.62 V can be ascribed to the lithiation of carbon matrices.[25,26] The CV curves almost completely overlap and exhibit one pair of redox peaks occurring at ~1.21/1.42 V in the subsequent cycles, indicating that the conversion reaction of Mo_2C with Li^+ is highly reversible and stable.[18,27] Fig. 5b presents the first galvanostatic charge/discharge curves of the samples. The initial discharge capacities of Mo_2C/C-1, Mo_2C/C-2 and Mo_2C/C-3 are 1203.1, 1057.3 and 931.8 mA h g^{-1} at 0.2 A g^{-1}, respectively, with coulombic efficiencies of 55.9%, 61.6% and 56.2%. Obviously, the electrochemical properties of the Mo_2C/C nanosheet composites are greatly affected by their carbon content. The discharge capacities of the samples become lager with reducing carbon content. Nevertheless, an optimal carbon content is necessary to get a high coulombic efficiency. Fig. S3† shows the charge/discharge curves of the various Mo_2C/C nanosheet composites at different cycles. The Mo_2C/C-2 exhibits a smallest voltage separation between the charge and discharge curves as compared to Mo_2C/C-1 and Mo_2C/C-3, revealing lowest electrochemical polarization, which could be ascribed to the fast ion and electron transport properties of the hierarchical nanosheet architecture.

Fig. 5c compares the cycling performance of the composites with various carbon contents. The Mo_2C/C-2 displays much higher capacity from the 60th cycle onwards as compared to Mo_2C/C-1 and Mo_2C/C-3. Interestingly, the capacities of Mo_2C/C-2 and Mo_2C/C-3 becomes larger during the cycling process. This may result from an electrochemical activation process of Mo_2C with the electrolyte gradually permeating into the nanosheet composites because of the existence of carbon with relative high content in those two composites. After 300 cycles, the reversible capacity of Mo_2C/C-2 reaches to 868.6 mA h g^{-1} with 133.4% capacity retention efficiency. Nevertheless, the similarly cycled Mo_2C/C-1 and Mo_2C/C-3 deliver reversible capacities of 566.7 and 586.2 mA h g^{-1}, which are 84.1% and 112.0% of their initial values, respectively. The morphological and structural

evolutions of the various Mo_2C/C nanosheet composites after cycling test were investigated in details through SEM analysis (Fig. S4†). The results demonstrate that the Mo_2C/C-2 exhibits best structural integrality and smallest volume change after cycling, which supports the excellent cycling stability of this material. Additionally, the electrochemical performances of p-C and Mo_2C/C-4 were investigated. As seen in Fig. S5a and c,† the p-C delivers low initial discharge (245.8 mA h g^{-1}) and charge (123.3 mA h g^{-1}) capacities and it maintains a reversible capacity of 121.2 mA h g^{-1} over 200 cycles. Though a relative high initial discharge capacity (1013.8 mA h g^{-1}) is achieved, the charge capacity is only 406.9 mA h g^{-1} for Mo_2C/C-4 (Fig. S5b and d†). After 200 cycles, the reversible capacity of Mo_2C/C-4 is 449.7 mA h g^{-1}, which is much lower than that of the similar cycled Mo_2C/C-2 (767.3 mA h g^{-1}).

The rate performance of the various Mo_2C/C nanosheet composites (over 300 cycles at 0.2 A g^{-1}) was explored at different current densities ranging up from 0.1 to 5.0 A g^{-1}. As displayed in Fig. 5d, the Mo_2C/C-2 reveals much higher capacity than Mo_2C/C-1 and Mo_2C/C-3 at every current density. The reversible capacities of Mo_2C/C-2 are 871.3, 803.9, 725.1, 661.3, 600.8 and 541.8 mA h g^{-1} at 0.1, 0.2, 0.5, 1.0, 2.0 and 5.0 A g^{-1}, respectively. Impressively, the Mo_2C/C-2 is still able to provide capacities of 699.9 and 818.2 mA h g^{-1} when coming back to 1.0 and 0.2 A g^{-1}, respectively, signifying favorable rate reversibility. In order to exploit its long-term cycling stability, the Mo_2C/C-2 was cycled at the high current density of 5.0 A g^{-1} (Fig. 5e). Though the capacity of Mo_2C/C-2 undergoes a declining process in the first 500 cycles, it increases to 532.1 mA h g^{-1} over 5000 cycles, with a capacity retention efficiency of 122.1%. We note this outstanding cycle life of Mo_2C/C-2 is superior to those of most other Mo_2C-based materials reported to date (Table S1†).[15,17–19,25,27–29] Meanwhile, the Mo_2C/C-2 exhibits high coulombic efficiencies of around 100% from the 30th cycle onwards, revealing that the lithium storage of this hierarchical nanosheet composite is highly reversible.

To deeply explore the lithium storage behavior, the lithium reaction kinetics of the hierarchical nanosheet composite was performed with the CV measurements at various sweep rates between 0.1 and 5.0 mV s^{-1}. As depicted in Fig. 6a, the Mo_2C/C-2 presents highly similar CV profiles and slight voltage delay with increasing the sweep rate, manifesting a fast pseudocapacitive lithium storage process that is independent of sweep rate. The total charge storage can be categorized into surface-controlled (capacitive) effect and diffusion-controlled (battery) process, and therefore the current response (i) and sweep rate (v) can be described as following relationship:[30,31]

$$i = av^b \quad (1)$$

$$\log(i) = b\log(v) + \log(a) \quad (2)$$

in which a/b are empirical parameters. The lithium storage behavior depends on the b-value, which derives from slope of the log(i) *vs.* log(v) plot. When the b-value is 0.5, a typical diffusion-controlled (battery) process can be identified. Whereas, the b-value of 1.0 suggests that the electrochemical

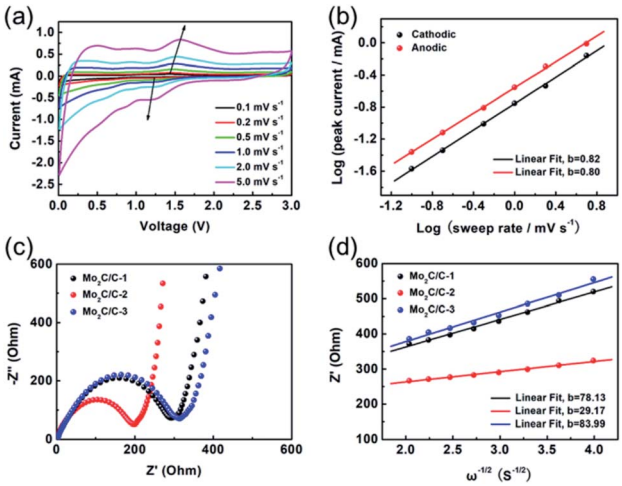

Fig. 6 (a) CV curves of Mo_2C/C-2 at sweep rates from 0.1 to 5.0 mV s^{-1}; (b) relationship between the peak currents and scan rates in their logarithmic format for Mo_2C/C-2; (c) Nyquist plots of Mo_2C/C-1, Mo_2C/C-2 and Mo_2C/C-3 at fresh coin cells; (d) corresponding linear fits of the Z' *versus* $\omega^{-1/2}$ in the low-frequency region.

reaction is determined with an ideal surface-controlled (capacitive) behavior. According to Fig. 6b, the b-values of cathodic peaks and anodic peaks for Mo_2C/C-2 are 0.82 and 0.8 respectively, which further demonstrates a typical pseudocapacitive behavior with fast lithium storage kinetics.

In addition, EIS analysis was carried out to understand the charge transport properties of the Mo_2C/C nanosheet composites. Fig. 6c depicts the Nyquist plots of Mo_2C/C-1, Mo_2C/C-2 and Mo_2C/C-3 at fresh coin cells. A depressed semicircle can be observed at high frequencies, which is related to the resistances of the charge transfer (R_{ct}) and SEI films (R_f). Meanwhile, the inclined line in low frequencies region is ascribed to Warburg-type resistance (W_1) corresponding to ion diffusion within electrode.[32,33] The equivalent circuit model shown in Fig. S6† can be used to fit the datum of the impedance spectra. The Mo_2C/C-2 electrode delivers a smallest R_{ct} value of 202.1 Ω (295.7 Ω for Mo_2C/C-1 electrode, 317.9 Ω for Mo_2C/C-3 electrode), indicating fastest interface charge transfer for this electrode.[8,34] This can be explained by the favorable electron transport between Mo_2C and carbon matrices in the hierarchical nanosheet architecture of Mo_2C/C-2. Fig. S7† displays the Nyquist plots of the various Mo_2C/C nanosheet composites during cycling test. Both the Mo_2C/C-2 and Mo_2C/C-3 exhibit much larger decline in the resistances of R_{ct} and R_f as compared to Mo_2C/C-1, indicating the existence of an obvious activation process during cycling, which supports the phenomenon of capacity increase for the Mo_2C/C-2 and Mo_2C/C-3. Additionally, the diffusion coefficient of Li^+ (D_{Li^+}) in the various Mo_2C/C nanosheet composites can be calculated from Warburg region using the formula (3):[35,36]

$$D_{Li^+} = R^2T^2/2A^2n^4F^4C^2\sigma^2 \quad (3)$$

$$Z' = R + \sigma\omega^{-1/2} \quad (4)$$

where R, T, F, A, n and C are the universal gas constant, the absolute temperature, the Faraday constant, the surface area of working electrode, the electrons number per molecule during redox reaction, the molar concentration of Li^+, respectively. Besides, σ is the Warburg factor, which is associated with Z' (formula (4)).[37,38] As seen in Fig. 6d, the σ was obtained from the slope of the fitting line of Z' and $\omega^{-1/2}$ in the Warburg region. The D_{Li^+} value of Mo_2C/C-2 is 2.59×10^{-10} cm^2 s^{-1}, which is much higher than those of Mo_2C/C-1 (3.61×10^{-11} cm^2 s^{-1}) and Mo_2C/C-3 (3.12×10^{-11} cm^2 s^{-1}). Consequently, the EIS results confirm the fast ion and electron transport properties of Mo_2C/C-2, which could be ascribed to the favorable charge transport pathways of the unique hierarchical nanosheet architecture.

Conclusions

In conclusion, we report a rational pyrolysis approach to synthesize Mo_2C/C nanosheet composites using cubic NaCl crystals as the templates. The morphology of the Mo_2C/C nanosheet composites can be controlled with the carbon content and a unique hierarchical architecture is obtained. The Mo_2C nanosheets exhibit a thickness of 40–100 nm and uniformly grow onto/into the carbon nanosheet matrices. This unique architecture can facilitate fast ion and electron transports between Mo_2C and carbon matrices and maintain good structural stability, thus resulting in high-performance lithium storage. As a consequence, the hierarchical Mo_2C/C nanosheet composite exhibits a reversible capacity of 868.6 mA h g^{-1} at 0.2 A g^{-1} over 300 cycles, and a high rate capacity of 541.8 mA h g^{-1} still can be achieved even at 5.0 A g^{-1}. Impressively, the hierarchical Mo_2C/C nanosheet composite demonstrates excellent cyclability with a capacity retention efficiency of 122.1% after 5000 successive cycles at 5.0 A g^{-1}. The high capacity and outstanding cycle life demonstrate the good application prospect in high-performance LIBs for the hierarchical Mo_2C/C nanosheet composite.

Author contributions

Xin Yue: data curation, writing – original draft; Minglei Cao: conceptualization, writing – review & editing, funding acquisition; Limeng Wu: data curation; Wei Chen: data curation; Xingxing Li: writing – review & editing; Yanan Ma: funding acquisition; Chuankun Zhang: writing – review & editing, supervision.

Conflicts of interest

There are no conflicts to declare.

Acknowledgements

Financial support from the National Natural Science Foundation of China (11904091), the Natural Science Foundations of Hubei Province (2019CFB375 and 2019CFB259), and the Doctoral Research Fund of HUAT (BK201807) are acknowledged.

Notes and references

1 J. M. Tarascon and M. Armand, *Nature*, 2001, **414**, 359.
2 J. W. Choi and D. Aurbach, *Nat. Rev. Mater.*, 2016, **1**, 1.
3 P. Yang and J. M. Tarascon, *Nat. Mater.*, 2012, **11**, 560.
4 A. Mukhopadhyay, A. Tokranov, X. Xiao and B. W. Sheldon, *Electrochim. Acta*, 2012, **66**, 28.
5 Y. F. Ma, H. C. Chang, M. Zhang and Y. S. Chen, *Adv. Mater.*, 2015, **27**, 5296.
6 P. Roy and S. K. Srivastava, *J. Mater. Chem. A*, 2015, **3**, 2454.
7 Y. Zhao, X. Li, B. Yan, D. Xiong, D. Li, S. Lawes and X. Sun, *Adv. Energy Mater.*, 2016, **6**, 1502175.
8 M. Cao, L. Tao, X. Lv, Y. Bu, M. Li, H. Yin, M. Zhu, Z. Zhong, Y. Shen and M. Wang, *J. Power Sources*, 2018, **396**, 327.
9 S. Fang, D. Bresser and S. Passerini, *Adv. Energy Mater.*, 2020, **10**, 1902485.
10 Q. Li, H. Li, Q. Xia, Z. Hu, Y. Zhu, S. Yan, C. Ge, Q. Zhang, X. Wang, X. Shang, S. Fan, Y. Long, L. Gu, G. X. Miao, G. Yu and J. S. Moodera, *Nat. Mater.*, 2021, **20**, 76.
11 X. Chen, Z. Kong, N. Li, X. Zhao and C. Sun, *Phys. Chem. Chem. Phys.*, 2016, **18**, 32937.
12 M. Q. Zhao, M. Torelli, C. E. Ren, M. Ghidiu, Z. Ling, B. Anasori, M. W. Barsoum and Y. Gogotsi, *Nano Energy*, 2016, **30**, 603.
13 Y. Zhong, X. Xia, F. Shi, J. Zhan, J. Tu and H. J. Fan, *Adv. Sci.*, 2016, **3**, 1500286.
14 Q. C. Zhu, S. M. Xu, M. M. Harris, C. Ma, Y. S. Liu, X. Wei, H. S. Xu, Y. X. Zhou, Y. C. Cao, K. X. Wang and J. S. Chen, *Adv. Funct. Mater.*, 2016, **26**, 8514.
15 Y. Zhu, S. Wang, Y. Zhong, R. Cai, L. Li and Z. Shao, *J. Power Sources*, 2016, **307**, 552.
16 W. Devina, J. Hwang and J. Kim, *Chem. Eng. J.*, 2018, **345**, 1.
17 L. Yang, X. Li, S. He, G. Du, X. Yu, J. Liu, Q. Gao, R. Hu and M. Zhu, *J. Mater. Chem. A*, 2016, **4**, 10842.
18 F. Lyu, S. Zeng, Z. Sun, N. Qin, L. Cao, Z. Wang, Z. Jia, S. Wu, F. X. Ma, M. Li, W. Wang, Y. Y. Li, J. Lu and Z. Lu, *Small*, 2019, **15**, 1805022.
19 H. Xin, Y. Hai, D. Li, Z. Qiu, Y. Lin, B. Yang, H. Fan and C. Zhu, *Appl. Surf. Sci.*, 2018, **441**, 69.
20 D. Wang, T. Guo and Z. Wu, *ACS Sustainable Chem. Eng.*, 2018, **6**, 13995.
21 X. Zeng, X. Gao, G. Li, M. Sun, Z. Lin, M. Ling, J. Zheng and C. Liang, *J. Mater. Chem. A*, 2018, **6**, 17142.
22 C. Wu and J. Li, *ACS Appl. Mater. Interfaces*, 2017, **9**, 41314.
23 D. Hou, S. Zhu, H. Tian, H. Wei, X. Feng and Y. Mai, *ACS Appl. Mater. Interfaces*, 2018, **10**, 40800.
24 B. Yu, D. Yang, Y. Hu, J. He, Y. Chen and W. He, *Small Methods*, 2019, **3**, 1800287.
25 M. Zhang, X. Huang, H. Xin, D. Li, Y. Zhao, L. Shi, Y. Lin, J. Yu, Z. Yu, C. Zhu and J. Xu, *Appl. Surf. Sci.*, 2019, **473**, 352.
26 T. Thomberg, A. Jänes and E. Lust, *Electrochim. Acta*, 2010, **55**, 3138.
27 L. Yang, X. Li, Y. Ouyang, Q. Gao, L. Ouyang, R. Hu, J. Liu and M. Zhu, *ACS Appl. Mater. Interfaces*, 2016, **8**, 19987.
28 X. Yang, Q. Li, H. Wang, J. Feng, M. Zhang, R. Yuan and Y. Chai, *Chem. Eng. J.*, 2018, **337**, 74.

29 X. Liu, Z. Li, S. Zhang, H. Long, H. Wei, H. Zhang, H. Li and C. Zhao, *Ceram. Int.*, 2017, **43**, 14446.
30 V. Augustyn, J. Come, M. A. Lowe, J. W. Kim, P. L. Taberna, S. H. Tolbert, H. D. Abruña, P. Simon and B. Dunn, *Nat. Mater.*, 2013, **12**, 518.
31 J. Ni, S. Fu, C. Wu, Y. Zhao, J. Maier, Y. Yu and L. Li, *Adv. Energy Mater.*, 2016, **6**, 1502568.
32 X. Li, G. Wu, X. Liu, W. Li and M. Li, *Nano Energy*, 2017, **31**, 1.
33 Y. Zhang, Y. Meng, K. Zhu, H. Qiu, Y. Ju, Y. Gao, F. Du, B. Zou, G. Chen and Y. Wei, *ACS Appl. Mater. Interfaces*, 2016, **8**, 7957.
34 M. Cao, L. Gao, X. Lv and Y. Shen, *J. Power Sources*, 2017, **350**, 87.
35 Y. Zhu, X. Xu, G. Chen, Y. Zhong, R. Cai, L. Li and Z. Shao, *Electrochim. Acta*, 2016, **211**, 972.
36 M. Yousaf, Y. Wang, Y. Chen, Z. Wang, A. Firdous, Z. Ali, N. Mahmood, R. Zou, S. Guo and R. P. S. Han, *Adv. Energy Mater.*, 2019, **9**, 1900567.
37 B. Luo, Y. Hu, X. Zhu, T. Qiu, L. Zhi, M. Xiao, H. Zhang, M. Zou, A. Cao and L. Wang, *J. Mater. Chem. A*, 2018, **6**, 1462.
38 Y. Xu, K. Chu, Z. Li, S. Xu, G. Yao, P. Niu and F. Zheng, *Dalton Trans.*, 2020, **49**, 11597.